Computational Study of Extrusion Bioprinting with Jammed Gelatin Microgel-based Composite Ink

Kaidong Song¹, Deming Zhang², Jun Yin², Yong Huang^{1,*}

¹ Department of Mechanical and Aerospace Engineering, University of Florida, Gainesville, Florida 32611, USA

² School of Mechanical Engineering, Zhejiang University, Hangzhou 310028, China

* Corresponding author: Department of Mechanical and Aerospace Engineering, University of Florida, Gainesville, FL 32611, USA, Phone: 001-352-392-5520, Fax: 001- 352-392-7303, Email: yongh@ufl.edu

Abstract

Material extrusion, a filament-based three-dimensional (3D) bioprinting technique, is commonly adopted to fabricate many complex constructs for its high efficiency, compatibility with a variety of biomaterials, and easy realization. During extrusion bioprinting, the morphology (including the shape and size) of extruded filaments is of great interest since the filaments are the basic building blocks for printed 3D structures and the filament morphology determines the printing resolution, surface quality, and part mechanical strength. The objective of this study is to computationally analyze the printing performance of the jammed gelatin microgel-based composite ink during extrusion in terms of the filament cross-sectional morphology and the influence of ink yield-stress fluid property on the structural printability. As seen from the rheological measurements, the jammed gelatin microgel composite ink is a viscoplastic fluid with the shear-thinning property, and its yield-stress fluid property enables it for self-supported printing applications. The ink printing process has been computationally modeled by using a fitted Herschel-Bulkley model to simulate the behavior of the jammed gelatin microgel composite ink for the first time, resulting in good modeling performance. In particular, the filament cross-sectional morphology under different printing conditions has been satisfactorily modeled. It is found that the cross-sectional shape turns flat rectangular under a small normalized gap distance (less than 0.6). Furthermore, the achievable maximum length (without collapse) of the jammed gelatin microgel-based composite ink,

deposited both between two supporting substrates and over a supporting substrate, has been satisfactorily estimated.

Keywords: Jammed, microgel, yield stress, three-dimensional printing, computational modeling

1. Introduction

Three-dimensional (3D) bioprinting techniques are being more extensively utilized for engineered tissue/organ fabrication applications by depositing and assembling cells and biomaterials into viable 3D constructs [1-3]. Included amongst the suitable bioprinting techniques are laser-induced forward transfer printing [4, 5], inkjet printing [6-8], and material extrusion printing [9-12]. Of these, material extrusion bioprinting is widely used to fabricate complex structures such as blood vessels, bones, cartilages, neural tissues, pharmaceutical delivery, and drug screening systems because of its high efficiency, compatibility with a variety of biomaterials, and easy realization.

During material extrusion, a filament printing process, materials are extruded onto a printing substrate through a nozzle and then rapidly solidify to ensure the fidelity of printed structures. Hydrogel materials, with their adjustable biochemical and biophysical properties and ability to provide a biocompatible extracellular matrix (ECM)-like microenvironment for living cells, have been favored for various tissue engineering applications for many years [13-16]. However, extrusion printing of hydrogel precursors is still an engineering challenge for tissue engineering applications [17, 18] since they need to be rapidly solidified to retain their shapes, which usually requires the use of additives or additional chemical modifications.

Generally speaking, fluids such as hydrogel solutions and suspensions can be classified into two general types according to the relationship between the shear rate and fluid viscosity: Newtonian fluids whose viscosity is shear rate independent and non-Newtonian fluids whose viscosity is a function of shear rate. For non-Newtonian fluids, the viscosity changes with the applied stress, and they have two main types: shear-thickening and shear-thinning fluids. Some of the non-Newtonian fluids are also viscoplastic fluids, which receive the most attention and usually have a minimum stress threshold for deformation known as the yield stress when being stressed. Due to the yield-stress fluid property, viscoplastic fluids can flow like a fluid when extruding through the nozzle

but rapidly stabilize as a solid to preserve the fidelity of the printed 3D structure, which meets the requirement for a self-supporting ink to fabricate freeform structures in air [12, 19].

To improve the printability of hydrogel materials without additives or chemical modifications, they can behave as viscoplastic fluids and be printable by using their corresponding jammed microgel format [12, 19, 20]. During conventional hydrogel material printing, liquid hydrogel precursor inks are deposited onto a target substrate and allowed to cross-link in situ. In a similar manner, for a jammed microgel system, the densely packed microgels are immobilized by surrounding microgels through their physical interactions, which results in a material that can be treated as a solid when viewed macroscopically. Interestingly though, when sufficient applied stress overcomes the restrictive/immobilizing force which restricts the motion of the microgels within the jammed system, the microgels move relative to one another with the whole system behaving as a liquid [21-24]. The system recovers immediately after the applied stress is reduced to below the yield stress of the jammed microgel system. In short, the jammed microgel system can flow and recover by responding to applied stress (gel-sol and sol-gel transitions), making jammed microgels ideal for use in extrusion printing without the need for additional solidification in order to retain printed structures in situ. This interesting yield-stress fluid property can minimize the immediate need for any cytotoxic cross-linking process during printing. In addition, it permits a longer time for slow-reaction cross-linking processes such as enzymatic cross-linking [25-27].

The objective of this study is to computationally analyze the printing performance of the jammed gelatin microgel-based composite ink during extrusion in terms of the filament cross-sectional morphology and the influence of ink yield-stress fluid property on the structural printability. Such a jammed composite ink has an interesting stress-dependent solid-liquid transition property as a non-Newtonian yield-stress fluid. Due to its good biocompatibility and biodegradability and suitable mechanical stiffness [28, 29], gelatin is used here to prepare the gelatin microgel-based ink. Computational experiments have been conducted to study the relationship between the printing conditions (gap height h and flow rate multiplier U/V) and filament morphology by using the Herschel–Bulkley model to capture the constitutive behavior of the jammed gelatin microgel-based ink for the first time. It is noted that the jammed gelatin microgel-based ink herein can be considered as an example of non-Newtonian viscoplastic fluids with the yield-stress fluid property,

which are utilized for 3D printing in air. The modeling accuracy has been validated by the experimental results, and the modeling approach has been further applied to evaluate the structure printability when using the jammed gelatin microgel-based ink.

2. Background

During extrusion printing of 3D structures, the ink printability is typically evaluated in terms of the filament morphology, surface quality, and part mechanical strength while the filament crosssectional morphology is of particular interest. Generally, the fabrication resolution depends on the cross-sectional morphology and size of extruded filaments since the extruded filaments are basic building units for material extrusion applications and each filament size determines the printing resolution [9]. Surface quality along the z direction is also influenced by the layer thickness [10, 30] which is typically selected according to the cross-sectional morphology of deposited filaments. When the layer thickness is too small, the subsequent filament overlaps with the previously deposited one, which leads to an over deposition phenomenon; a larger layer thickness leads to a fractured structure. In addition, the part mechanical strength is related to the contact area between two adjacent filaments, which is dependent on the filament cross-sectional morphology. For a layer-by-layer fabrication process, the cross-sectional morphology of filaments is critical to the bonding strength between two adjacent filaments, which decides the bonding area [31-33]. It is noted that the hatch distance and resulting infill density are also important to the surface quality along the xy plane. Furthermore, the knowledge of the filament cross-sectional morphology allows better control of part mechanical properties when printing structures with anisotropic mechanical strength [34, 35]. Therefore, it is of great importance to investigate the filament morphology during extrusion printing, which is the subject of this study.

The filament morphology during extrusion printing can be studied experimentally or computationally, with computational modeling as a predictive tool providing an alternative approach to understanding and guiding the extrusion printing process. Material extrusion printing process has been studied computationally using both two-dimensional (2D) [36, 37] and 3D [38-42] models. In addition to some macroscopic mechanical analysis studies [43, 44], the material extrusion printing process has been computationally modeled in terms of the heat transfer process [39], material residual stresses [40], structure microarchitectures [41], and filament morphology

[42]. In particular, D'Amico et al. [39] have simulated the heat transfer process during material extrusion and the effect of printing speed on the temperature. Brenken et al. [40] have predicted the residual stress of printed structures due to the material anisotropy and printing process. Gleadall et al. [41] have utilized a volume conserving model (VOLCO) to predict the microarchitecture of printed porous scaffold structures. In terms of the filament morphology, Comminal et al. [42] have used a Newtonian fluid model to study the dependency of its cross-sectional morphology and printing force on the printing speed and/or layer thickness. While most of the current computational simulation studies on extrusion printing have been performed under the assumptions of a Newtonian fluid [42, 45, 46], some works have used a non-Newtonian powerlaw [37] or Carreau fluid model [47, 48] to conduct computational simulations, which cannot represent the yield-stress fluid property [12], the most important rheological property of microgelbased inks, which are of interest in this study. While non-Newtonian models such as the Herschel-Bulkley model have been utilized, they have only been used to predict the shear rate and velocity distribution [49] or control the flowrate [50] during printing. As such, accurate modeling of microgel ink printing still calls for an improved modeling approach that can capture the unique yield-stress fluid property of microgel-based inks for process planning, which is the subject of this study. It is noted that the jammed composite ink herein is a representative non-Newtonian yieldstress fluid, so the studied approach is also applicable to the modeling of other yield-stress fluids during material extrusion printing.

3. Preparation and characterization of jammed microgel-based ink

3.1 Preparation of jammed microgel-based ink

For jammed microgel-based ink preparation, a complex coacervation process was used to get gelatin-based microgels with smaller size and more uniform shape. Briefly, 2.0% w/v gelatin (100 bloom type B, Fisher Scientific, Hampton, NH), 0.25% w/v F127 (Pluronic, Sigma-Aldrich, St. Louis, MO), and 0.1% w/v gum Arabic (Acacia gum, Sigma-Aldrich, St. Louis, MO) were dissolved in a 50% v/v ethanol solution (Ethanol 200 Proof, Decon Labs, King of Prussia, PA) at 50 °C and adjusted to 7.50 pH by addition of aqueous 50% v/v sodium hydroxide (NaOH, Sigma-Aldrich, St. Louis, MO). The beaker was then placed under an overhead stirrer (Fisher Scientific, Hampton, NH) set to 500 rpm to mix overnight and then allowed to cool to room temperature to form the slurry of gelatin-based microgels. Parafilm was used to seal the beaker to minimize

evaporation. Transglutaminase (TG) (Moo Gloo TI Transglutaminase Formula, Modernist Pantry, York, ME) powders were dissolved in deionized (DI) water, mixing thoroughly using a vortex mixer (Mini Vortexer, Fisher Scientific, Hampton, NH). The mixed TG solution was then incubated in a bead bath for 30 minutes at 37 °C to get a 20.0% w/v (TG) solution stock. To get a final concentration of 1.0% w/v TG, the TG solution was added to the gelatin-based microgel slurry at a 19:1 ratio using the overhead stirrer at 500 rpm for chemical cross-linking for one day. The resulting slurry was collected into 50 mL conical tubes and centrifuged at 1500 rpm for 5 minutes to remove supernatant and compact cross-linked microgels. To deactivate the crosslinking agent TG in the prepared microgels, the 50 mL conical tube packed with the gelatin-based microgels was put in 100 °C boiling water for 20 minutes. Then the microgels were resuspended in DI water to wash away ethanol and Pluronic F127. The gelatin-based microgel slurry was further processed three times using a centrifuge (5804 R, Eppendorf, Hamburg, Germany) with 1500 rpm for 5 minutes followed with 4200 rpm for 10 min to eliminate extra water. The collected gelatin microgels were mixed with gelatin dry powders at 3% w/v as in a previous study [12]. The mixture was blended with a vortex mixer thoroughly and then incubated in a bead bath incubator at 37 °C for 30 minutes until the gelatin powders were completely dissolved. The resulting composite was stored at 4°C and recovered to room temperature before use.

For comparison, a pure 5% w/v gelatin solution was used as a Newtonian fluid to investigate the significance of the yield-stress fluid property of the jammed gelatin microgel-based ink on the printing performance. The 5% concentration was selected based on the 2% gelatin microgel and 3% gelatin solution used for the preparation of the jammed gelatin microgel composite ink. Specifically, the gelatin solution was prepared by dissolving proper amount of gelatin dry powders in DI water and incubated in a bead bath at 37 °C until they were completely dissolved.

3.2 Determination of ink rheological properties

To analyze the rheological properties of the jammed gelatin microgel-based composite ink and gelatin solution, a rheometer (MCR-702 TwinDrive, Anton-Paar, Graz, Austria) with a 25 mm sandblasted ($Ra = 4.75 \mu m$) parallel-plate measuring geometry and 1 mm gap was utilized to perform all rheology measurements. Steady rate sweeps were conducted at a low strain (1%) for a shear rate range from $0.1 \, s^{-1}$ to $100 \, s^{-1}$ to detect the fluid viscosity and yield stress, if have.

To get the surface tension of the jammed gelatin microgel composite ink and gelatin solution (both in air) for computational simulations, a tensiometer (Attension ThetaLite 101, Biolin Scientific, AB, Sweden) was used to characterize the resulting droplets under different situations based on the pendant drop tensiometry.

4. Extrusion bioprinting setup and implementation

4.1 Extrusion bioprinting setup

To describe the filament deposition process during extrusion printing, a schematic of material extrusion process and the related computational model are illustrated in Figure 1a and 1b, respectively. The extrusion nozzle is simplified as a cylindrical tube with an inner diameter of D, which is placed above a substrate by a gap height (stand-off distance) h, the gap height is always considered as the layer thickness. As for the extrusion printing process shown in Figure 1b, the simulation model is set up as symmetrical with respect to a middle vertical plane of the nozzle in the printing direction, thus the entire modeling domain is cuboid, and the size is 6 mm × 2.5 mm × 3 mm. The remaining external surfaces of the numerical modeling domain are outlet boundaries, where the material is free to exit. Under the assumption that the flow at the nozzle exit is fully developed and laminar, the influence of nozzle length is neglected for the flow exiting the nozzle. Since the input-output volumetric flowrate is conserved, a relationship can be set up among the printing head velocity V, nominal filament cross-sectional area S, average velocity inside the nozzle U, and inner cross-sectional area of extrusion nozzle as follows [45]:

$$VS = U\frac{\pi D^2}{4} \tag{1}$$

The stand-off distance h also affects the printing quality and filament cross-sectional area S during printing the jammed microgel-based inks. Herein, the filament cross-sectional morphology is characterized by two dimensionless parameters: the normalized stand-off distance h/D and the velocity ratio or flow rate multiplier U/V. The material flow rate is determined automatically according to parameters set in the ball-screw-based printer used in this work, including V, D, h, and U/V. Through adjusting U/V, the amount of extruded materials can be tuned to get overdeposited (U/V is high) or undersized (U/V is low) filaments. For filament cross-section analysis, 15 different groups of h/D and U/V combinations are analyzed and measured using both

computational simulations and actual experimentation. The operating parameters selected for printing and computational simulations are listed in Table 1.

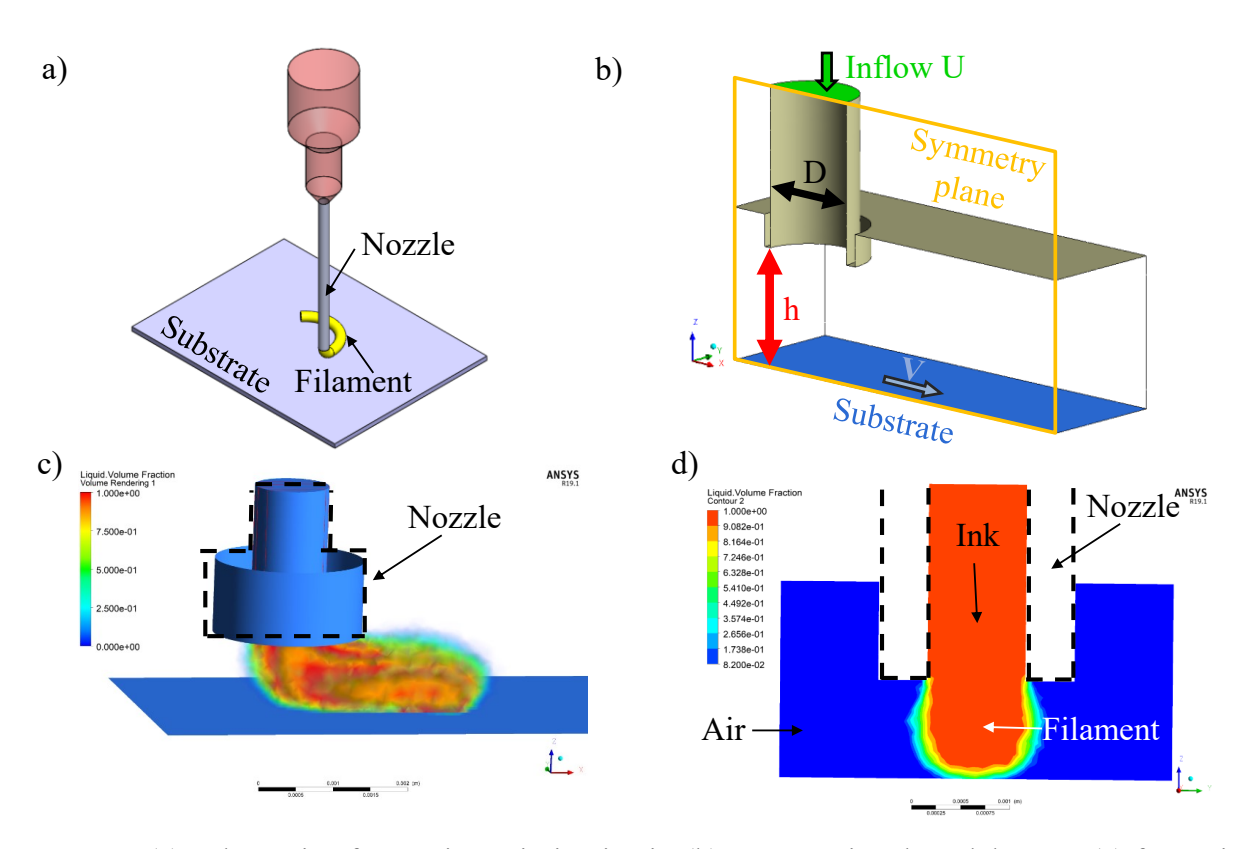


Figure 1. (a) Schematic of extrusion printing in air, (b) computational model setup, (c) front view of a simulation of filament deposition, and (d) side view of a simulation of filament deposition.

Table 1. Printing and simulation conditions.

Variable	Symbol	Unit	Value
Gap height (stand-off distance)	h	mm	0.62, 0.92, 1.23, 1.54, 1.85
Nozzle inner diameter	D	mm	1.54
Normalized gap height (ratio)	h/D	None	0.4, 0.6, 0.8, 1.0, 1.2
Flow rate multiplier (ratio)	U/V	None	1.0, 1.5, 2.0
Extrusion temperature	T	$^{\circ}\mathrm{C}$	25

4.2 Extrusion bioprinting system and printing protocols

All printing work was conducted using a 3-axis ball screw motion-controlled 3D material extrusion printer (Hyrel Engine SR, Hyrel3D, Norcross, GA). For filament cross-section analysis and filament-based structure deposition (self-supported filament and cantilever filament), the prepared microgel composite and gelatin solution ink were extruded using a 14-gauge nozzle (1.54 mm inner diameter, EFD Nordson, Vilters, Switzerland) with a path speed of 2 mm/s. Printing path codes were generated manually as custom G-code scripts.

4.3 Characterization of filament morphology

The filaments were cut through filaments printed on a glass slide using a surgical knife, and the cutting direction was perpendicular to the direction of printing. The filament cross-sections were determined using an optical microscope (Stereomaster, Fisher Scientific, Waltham, MA) combined with a digital optical microscope camera (Summit K2, OtixCam, China). The cross-section morphology of the printed filaments was analyzed using ImageJ (NIH, Bethesda, Maryland).

5. Computational simulation setup

In this study, a computational fluid dynamics (CFD) approach was conducted to evaluate the printability of the jammed microgel-based ink during extrusion printing in terms of the filament cross-sectional morphology and ink yield-stress fluid property using ANSYS® Fluent 19.0 (Ansys, Canonsburg, PA). The simulation model was set up as symmetrical with respect to the middle plane of the nozzle in the printing direction as shown in Figure 1b. For computational efficiency, only half of the geometry was simulated. To guarantee the precision of the computational simulation, the geometry was meshed using tetrahedrons, and the maximum size of the control volumes was set as 0.05 mm, resulting in 581791 elements. The time-step interval was 0.0001 s, and the max iteration/time step was 40 in all simulations. The initial speed of the substrate was 2 mm/s, the air volume fraction in this model was 100%, and the ink inflow from the top of the nozzle had a constant speed (2, 3, or 4 mm/s). The printing process of both the jammed microgel composite and gelatin solution inks was conducted under the following assumptions:

- (a) Both inks were considered incompressible, and
- (b) The interface condition between each ink and its counterpart (the surfaces of the receiving substrate and nozzle) was no slip.

For more intuitive understanding, the representative images of the printed whole filament and the cross-section of filament are shown in Figure 1c and 1d, respectively during the computational simulation process. The filament cross sections were measured 0.5 mm from the nozzle exit. The color distribution means the ink volume fraction, where the blue means the ink volume fraction as 0% and the red means the ink volume fraction as 100%. Herein, a 70% volume fraction threshold was used to generate the filament cross sections.

6. Extrusion printed filament cross-sectional morphology analysis

6.1 Constitutive model of jammed microgel-based ink

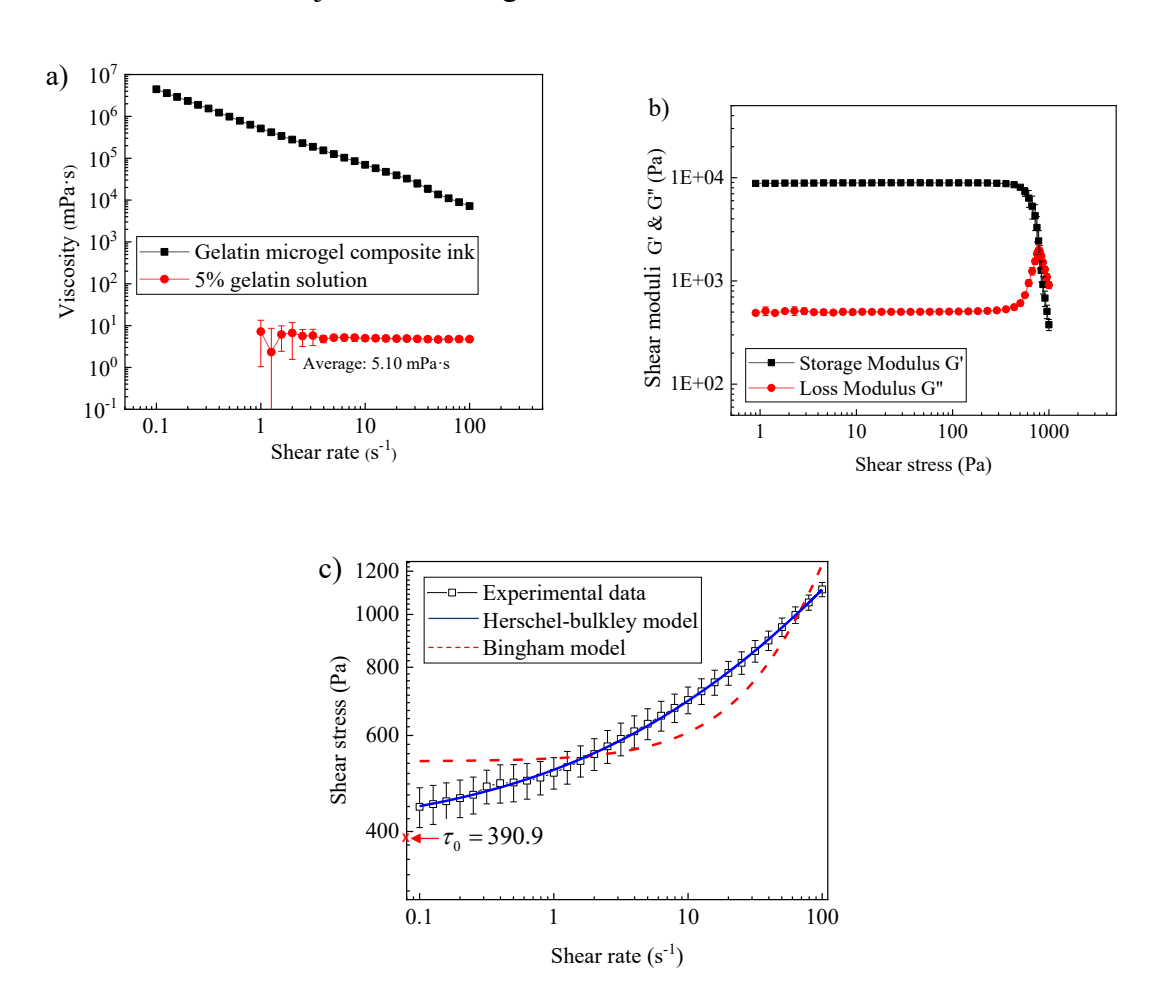


Figure 2. Rheological data of jammed microgel-based composite ink and gelatin solution. (a) Viscosity versus shear rate with a log scale, (b) shear moduli as a function of shear stress, and (c) shear stress versus shear rate.

As shown in Figure 2a, the jammed gelatin microgel composite ink is shear-thinning non-Newtonian fluid while the gelatin solution has a viscosity being independent of shear rate as a Newtonian fluid under relatively low shear rates (below 1000 s⁻¹) as reported before [51, 52]. The gelatin composite ink is a viscoplastic non-Newtonian fluid with yield stress as seen from Figure 2b in addition to being shear thinning. For accurate modeling of extrusion printing using the composite ink, a suitable viscoplastic shear-thinning non-Newtonian model should be utilized in order to better capture the rheological properties of the composite ink. The Bingham model is considered as the simplest viscoplastic non-Newtonian model, which uses a linear relationship between the shear stress and shear rate as follows:

$$\tau = \tau_0 + k\dot{\gamma} \tag{2}$$

where τ is the shear stress, γ is the shear rate, τ_0 is the yield stress, which can be determined by the extrapolated y-axis intercept, and k is the consistency index. The Herschel-Bulkley model is another viscoplastic non-Newtonian model, which combines the yield-stress effect of the Bingham model and the shear-thinning (or shear-thickening) behavior of power-law fluids:

$$\tau = \tau_0 + k\dot{\gamma}^n \tag{3}$$

where n is the flow index. If $\tau < \tau_0$ the composite ink behaves as a solid. If not, the composite ink behaves as a fluid. For n < 1, the fluid is shear-thinning, whereas n > 1, the fluid is shear-thickening.

Both the Bingham and Herschel–Bulkley models are fitted based on and compared with the experimental rheology data (Figure 2c) of the jammed gelatin microgel-based ink. The Herschel–Bulkley model is chosen as the constitutive model for the jammed gelatin microgel ink since it is more consistent with the rheology data based on the coefficient of determination analysis (R^2) (the Bingham model with a R^2 of 0.878 and the Herschel–Bulkley model with a R^2 of 0.999), and the resulting Herschel–Bulkley model is $\tau = 390.9 + 128.3\dot{\gamma}^{0.374}$.

Microstructure wise, the non-Newtonian jammed gelatin microgel-based composite ink studied here consists of monodisperse granular cross-linked microgels (TG cross-linked gelatin) dispersed in a solution phase (gelatin solution). As needed, living cells can be easily included in the solution

phase of the composite ink as described in a previous study [12]. The polymeric particles (microgels) are obtained by a complex coacervation process. Granular microgels are a collection of materials consists of distinct, viscoelastic hydrogel microparticles (HMPs). The diameter of the HMPs is generally greater than 10 µm. When the particle diameter is greater than this size, the gravitational forces on those HMPs are relatively higher than thermal forces. Additionally, because the inter-particle frictional force is much higher than the van der Waals force between neighboring microgels, the van der Waals force can be ignored here. These granular microgels are different from particulate matter, such as colloidal gels, due to their special properties: the existence of interparticle friction, lack of thermal motion, and relatively larger particle size (Figure 3a). Owing to these unique features, for granular microgels in a jammed state, the packed disordered microgels can transfer from a 'liquid-like' state to a 'solid-like' state when the particle-to-volume ratio is higher than 0.58 which is defined as 'random loose packing'. When granular microgels are more concentrated and higher than random loose packing, especially closer to a particle-to-volume fraction of 0.64 (defined as 'random close packing'), they can be treated as a solid which possesses all properties of conventional hydrogels [53]. Herein the jammed microgel composite ink has a particle-to-volume fraction around 0.8 as determined based on the volume change after being centrifuged, and this value is higher than 0.64 because the gelatin microgels are deformable and irregular. Interestingly, this densely packaged bulk remains flexible in air, responds as displace particles under an application of sufficient stress [54, 55], and recovers to a whole bulk after the removal of the applied stress (Figure 3b). This reversible transition between the 'solid-like' and 'liquid-like' states enables the jammed viscoplastic non-Newtonian ink as a good self-supporting ink for printing whose constitutive behavior can be adequately described using the Herschel-Bulkley model for the computational simulation purpose.

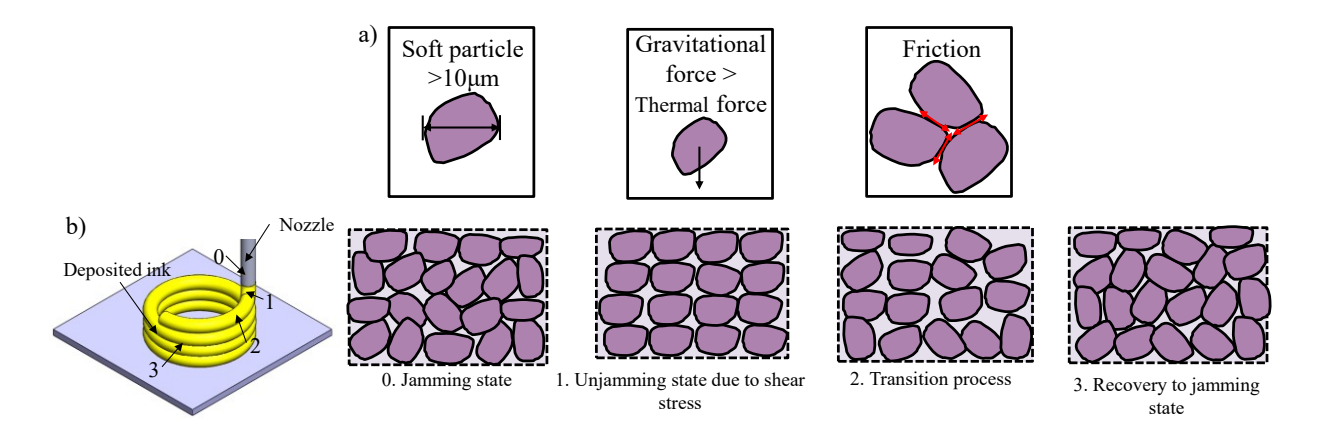


Figure 3. Overview of jammed granular microgel ink. (a) Properties for hydrogel microparticles, and (b) reversible transition of jammed microgel-based composite ink during extrusion printing.

6.2 Computational modeling fidelity using the Herschel-Bulkley model

Computational studies were performed using the Herschel–Bulkley model as the constitutive model as well as the Newtonian model during extrusion printing of the jammed gelatin microgel composite ink. The related material properties needed for computational studies are listed in Table 2. Specifically, filaments were deposited with U/V = 1.0 and h/D = 1.0. The modeling results are used to provide a qualitative comparison in terms of the printability as seen from the experimental and simulation results.

Table 2. Parameters used in the computational simulations.

Parameter	Definition	Value	Unit
$ au_0$	Yield stress of the jammed microgel composite ink	390.9	Pa
k	Consistency of the jammed microgel composite ink	128.3	Pa·s
n	Index of the jammed microgel composite ink	0.374	None
$\rho_{\it Composite}$	Density of the jammed microgel composite ink	1.07	g/cm ³
U	Average ink velocity inside the nozzle	2–4	mm/s
V	Printing head velocity	2	mm/s
$\rho_{_{Solution}}$	Density of the gelatin solution	1.05	g/cm ³
$\mu_{Solution}$	Viscosity of the gelatin solution	5.1	mPa·s

II.a. v	Eigen-viscosity of the jammed microgel composite ink	5×10 ⁵	mPa·s
μ _{Composite}	for simulation purpose		
$\gamma_{Solution}$	Surface tension of the gelatin solution in air	65.58	mN/m
$\gamma_{Composite}$	Surface tension of the jammed microgel composite ink	4.46	mN/m
	in air	4.40	
D	Inner diameter of the nozzle	1.54	mm
OD	Outer diameter of the nozzle	1.83	mm
h	Gap height (stand-off distance)	0.616-1.848	mm
$g_{0}^{}$	Gravitational acceleration	-9.81	m/s^2

Simulated and experimental cross-sectional morphologies of the jammed microgel composite are shown in Figure 4. The Herschel-Bulkley model (Figure 4a) is closer to the experimental result (Figure 4c) than the Newtonian model (Figure 4b). Due to the effect of yield-stress fluid property, a deposited filament from the jammed microgel composite ink can hold itself in air with an elliptical shape. When simulated using the Newtonian model, the cross section collapses, resulting in a half oval shape. The filament cross-section width (W) and height (H) as simulated by using the Herschel–Bulkley model are compared with those as measured in Figure 4d, demonstrating good modeling accuracy of the proposed computational study.

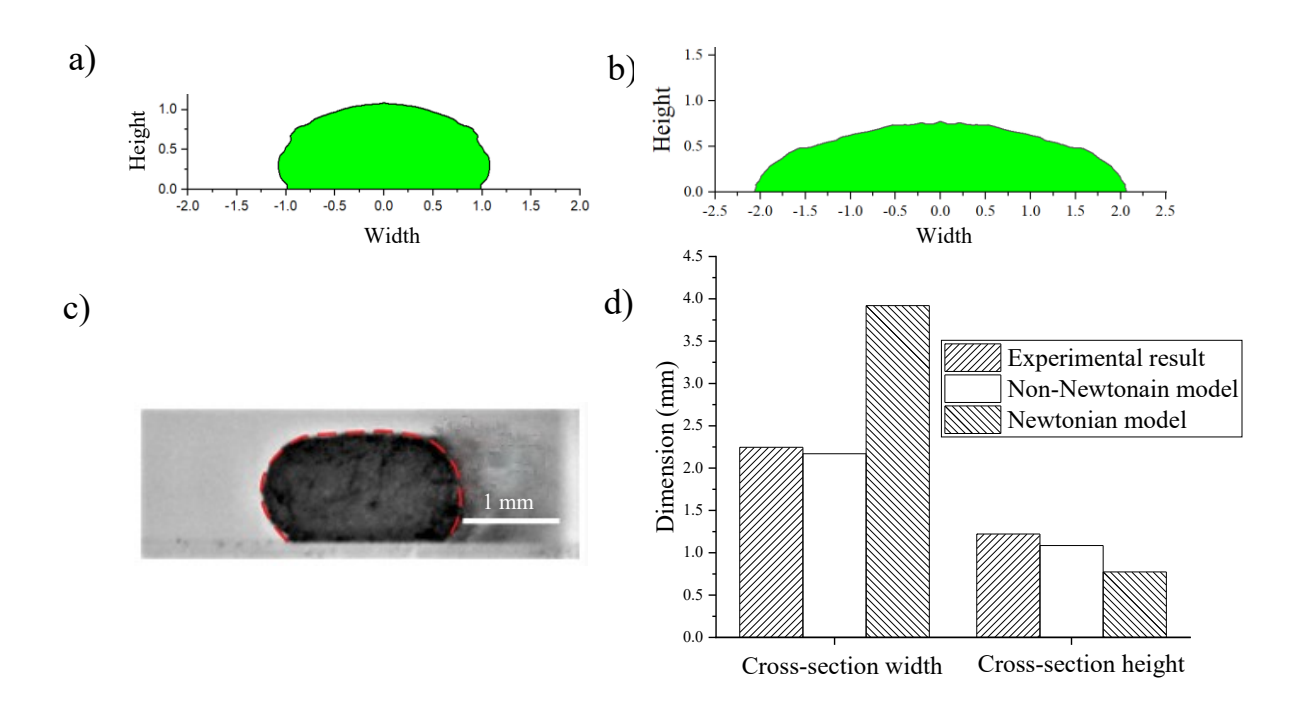
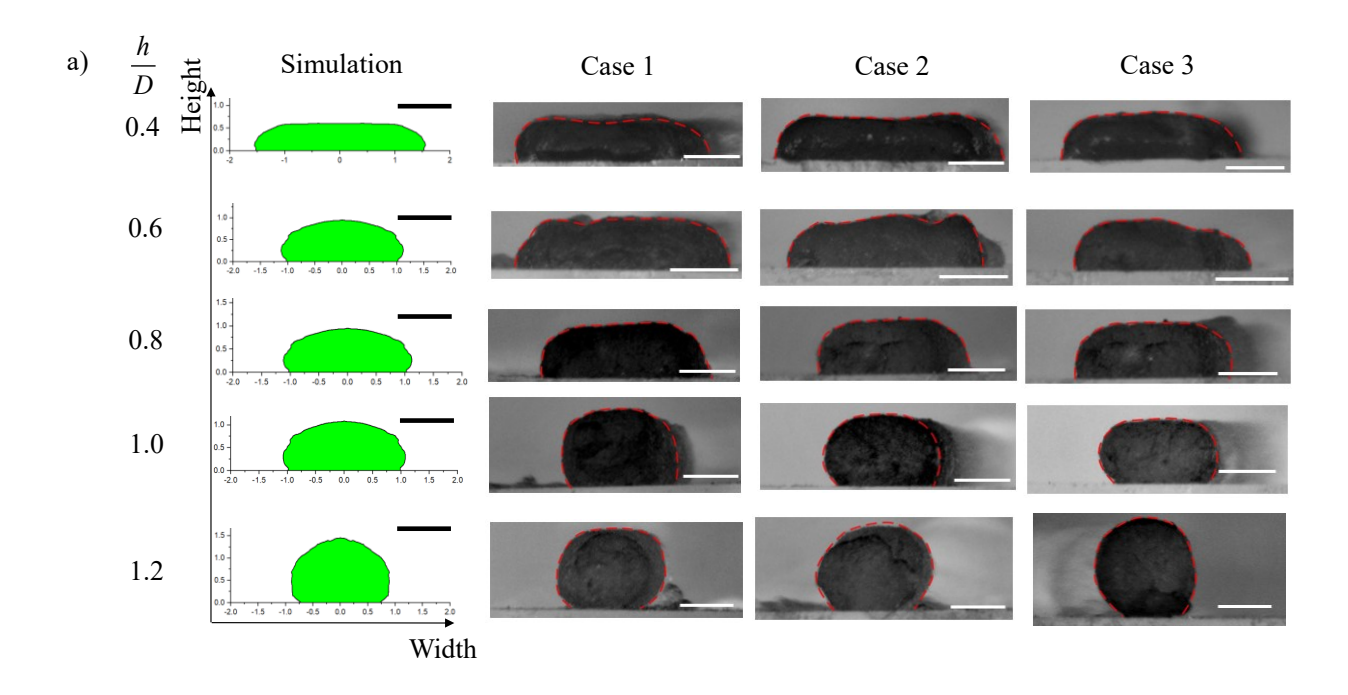


Figure 4. Cross-section morphology of filaments. (a) Simulation the Herschel–Bulkley model, (b) simulation result based on the Newtonian model, and (c) experimental result (U/V = 1.0 and h/D = 1.0) (red dashed line indicates the filament contour). (d) Dimensional comparison in terms of filament cross-sectional height and width.

6.3 Evaluation of the effects of printing conditions on filament cross section

To evaluate the effects of printing conditions on the filament cross-sectional morphology, the morphologies were measured, simulated, and compared under different U/V and h/D conditions. The computational simulation results under each condition are listed in the first graphical column of Figure 5 and three corresponding experimental cross-section contours are shown in the next three graphical columns, further confirming the modeling accuracy. As shown in all figures, with the increase of normalized gap height h/D, the cross-section morphology changes from rectangular with round corners to an increasingly circular shape. When h/D is 1.2, meaning that the gap height is larger than the nozzle diameter, the cross section is almost circular under U/V = 1.0. Under other flow rate and gap height combinations, the top of the cross sections may be flattened by the dispensing nozzle. With the increase of U/V from 1.0 to 1.5 to 2.0, which means more and more material is extruded out through the nozzle, the cross-sectional area becomes larger and larger.

Generally, the cross sections of deposited filaments during extrusion printing are simplified as elliptical [56] or circular [10]. This simplification may not hold during the printing of the jammed microgel composite ink under a small normalized gap distance (h/D < 0.6) since the cross-sectional shape is flat rectangular. For h/D = 0.4 with either U/V = 1.5 or U/V = 2.0, since there is too much material extruded out and the gap distance is too small, the deposited filaments have a side flow, and there is an observable dent in the middle of each filament; such printing conditions should be avoided.



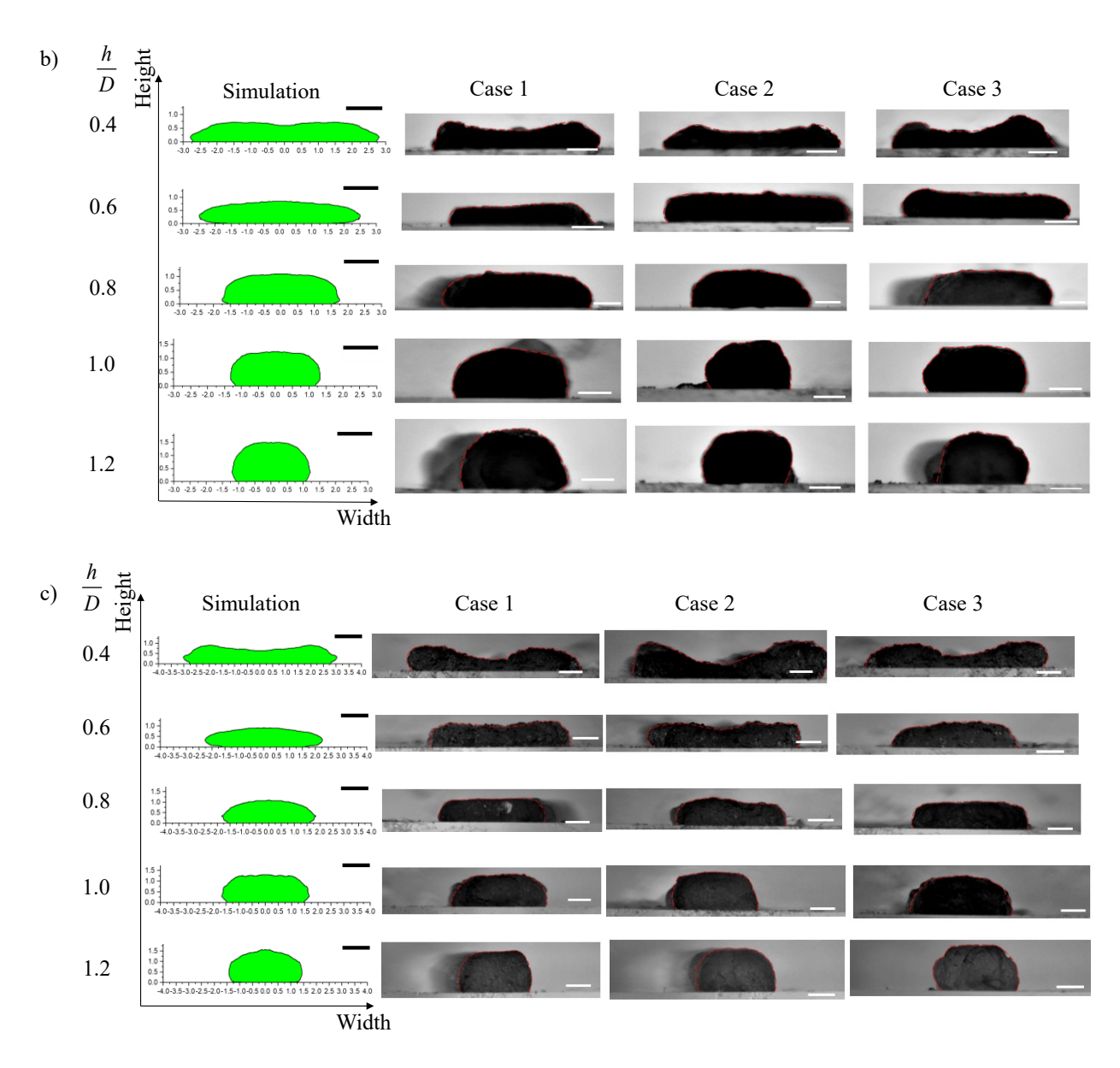


Figure 5. Filament cross-section morphology from computational simulation and experimental triplicate results under different printing conditions (a) U/V = 1.0, (b) U/V = 1.5 and (c) U/V = 2.0 (scale bar = 1 mm) (red dashed line indicates the filament contour).

To quantitatively compare the filament cross-section contour dimensions, their computational and experimental results are represented in terms of the cross-sectional height H (Figure 6a-c) and width W (Figure 6d-f). For those filaments with a dent in the middle, the height H was measured according to the height of the dent. Both computational and experimental results show that H increases but W decreases with the increase of h/D. The simulated cross-sectional width and height

slightly underestimate the measurement results, and this underestimation can be compensated by fine-tuning the ink volume being dispensed if needed.

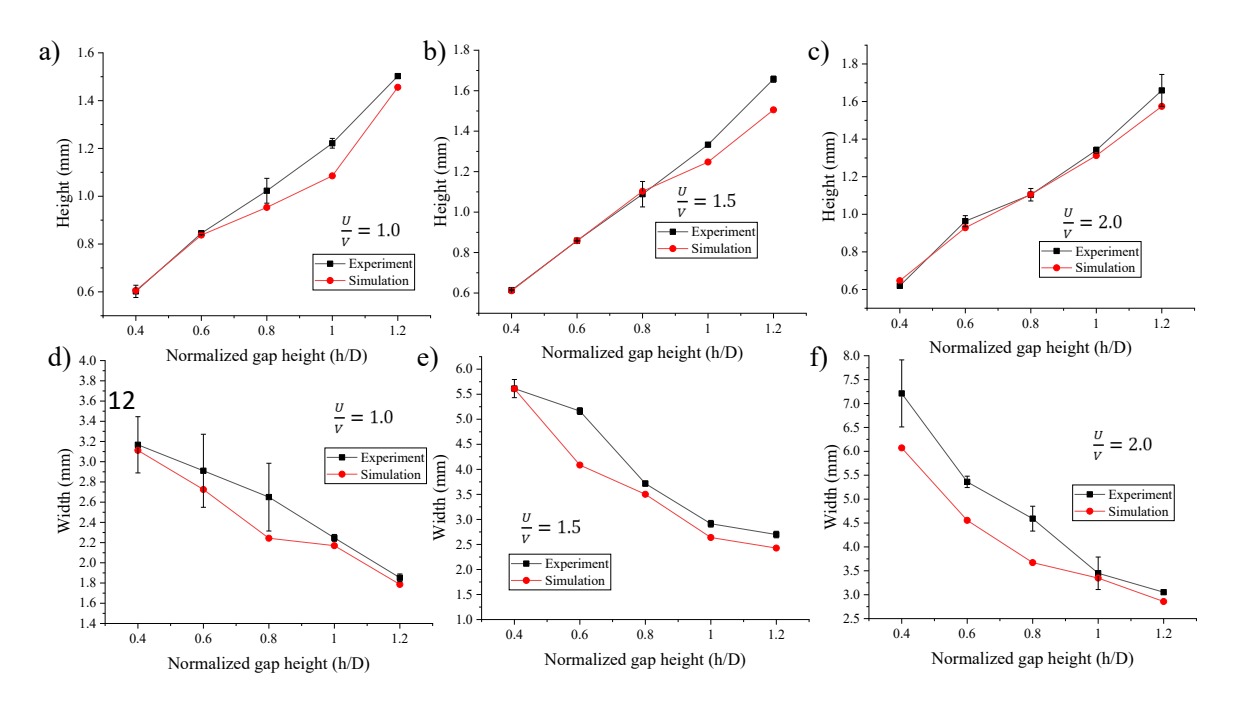


Figure 6. Simulated and printed cross-sectional heights (a-c) and widths (d-f)

6.4 Assessment of optimal vertical and horizontal printing overlaps

During extrusion printing, a subsequently deposited filament overlaps with a previously deposited filament horizontally or vertically. Figure 7a shows a typical filament (W = 2.17 mm and H = 1.09 mm as simulated) printed under U/V as 1.0 and h/D as 1.0, and Figure 7b, 7c, and 7d show different overlap situations with a vertical (z) or horizontal (x) distance at which the nozzle moves between adjacent layers/features in order to print a 3D structure. If the overlap distance is too large, the whole structure may have poor mechanical properties due to the weak connecting force between adjacent filaments/layers as shown in Figure 7b. If the overlap distance is too small, the subsequently printed layer overlaps with the previously deposited layer (Figure 7c), and the resulting over-deposition phenomenon can be obvious as accumulated after several layers. To make sure the structure has enough mechanical stiffness and minimize the over-deposition phenomenon, the overlap distance must be carefully selected. Generally, the cross section of deposited filaments is simplified as a perfectly circular or elliptical shape, which may introduce

some process planning errors as discussed before during printing of the jammed microgel composite ink since the cross-sectional shape may be elliptical or rectangular with different widths and heights under different printing conditions. A suitable overlap should make a printed structure with a good fusion between filament/layers which results in good mechanical strength. Herein the optimal overlap distances are determined when the filaments are tangent to those of adjacent layers in the vertical direction (z = H) but overlap with those in the same layer in the horizontal direction (z = 0.7W) (Figure 7d).

To validate the proposed overlap selection, a plate structure (length 20 mm, width 10 mm, and height 6 mm) was designed (Figure 7e) and printed using three different overlaps as shown in Figure 7g, 7f, and 7h. When both the horizontal and vertical overlaps are set equal to the filament width as x = z = W, the distance between two adjacent layers is too large, and the inter-layer connection is weak. As a result, the deposited layers can be clearly seen and are laminated (Figure 7f). When the horizontal and vertical overlaps are set to the filament height (x = z = H), the overdeposition phenomenon occurs, and the nozzle may be trapped in the printed layers and damage previously deposited filaments for this particular case (Figure 7g). As shown in Figure 7h, when the optimal overlaps (x = 0.7W and z = H for this particular case) are implemented, the printed structure has a well-controlled geometry and smooth surface, and the filaments integrate well with each other at the same and different layers. For process planning purpose, both W and H values can be determined computationally as described before while using the non-Newtonian Hershel-Bulkely model.

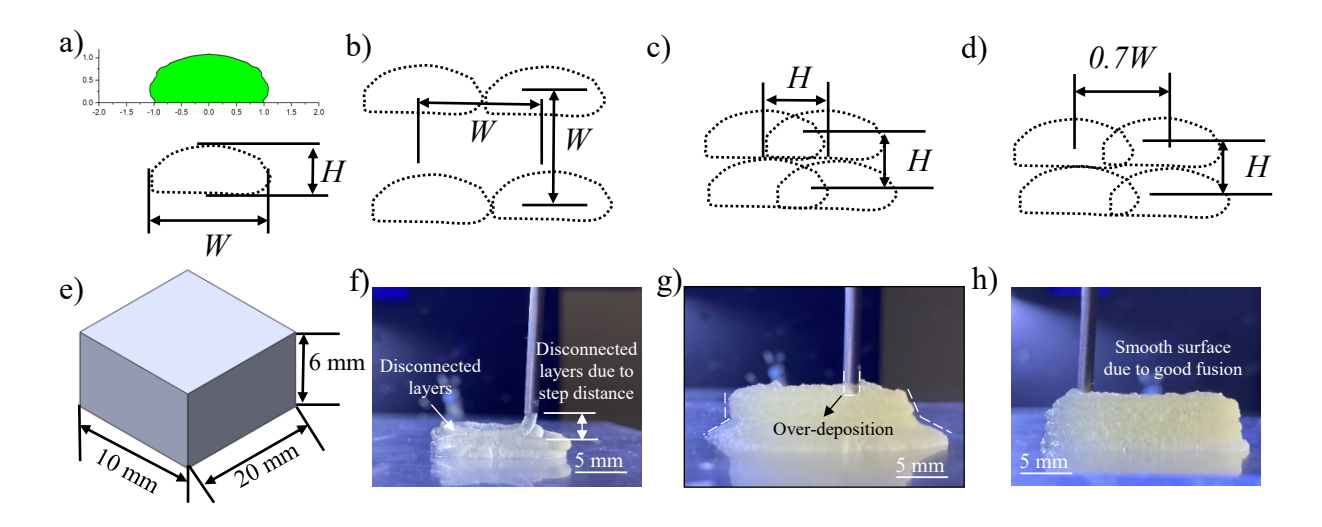


Figure 7. Printing overlap selection. a) Filament cross section with a height of 1.09 mm and a width of 2.17 mm (simulated and its schematic). b) Overlap distances along the vertical and horizontal directions set the same as the width of filament. c) Overlap distances along the vertical and horizontal directions set the same as the height of filament. d) Overlap as the filament height along the vertical direction and 30% overlap in the horizontal direction. e) Schematic of the designed plate structure. f) Printing with x = z = W = 2.17 mm (weak connection). g) Printing with x = z = H = 1.09 mm (over-deposition). h) Printing with x = 0.7W and z = H (good structure).

7. Analysis of self-supported printing property

In addition to the analysis of filament cross-sectional morphology, the structural printability of the jammed gelatin microgel composite ink should also be investigated. Since the simulation of entire structure printing is not of interest in this methodology study, the printing of complex structures is not simulated. The simulations were implemented based on the printing of a simply supported beam/filament (Movies M1) and a cantilever beam/filament as shown in Figures 8 and 9, respectively. Both were printed under U/V as 1.0 and h/D as 1.0 and simulated using the Herschel–Bulkley model. For comparison, the 5% gelatin solution was also printed and simulated using the Newtonian model as specified in Table 2. Printing of simply supported gelatin microgel and gelatin solution beams/filaments was also recorded (Movie M2).

7.1 Simply supported filament printing

For printing of a simply supported beam, when the jammed gelatin microgel composite ink is extruded without any support, it can be switched from the sol state to the gel state immediately. As a result, a self-supported filament can be formed which can hold its shape in air as observed (Figure 8a-1) as well as simulated (Figure 8a-2). In contrast, the gelatin solution is not a yield-stress material, so the viscous filament cannot bear any transverse shear stress due to the gravity effect when the filament is extended unsupported (beyond the edge of the supporting substrate). Instead, it breaks as illustrated in Figure 8b-1 and 8b-2. It is the yield-stress fluid property instead of the high viscosity that enables the non-Newtonian jammed gelatin microgel composite ink to be printed unsupported. The mechanics of such a simply supported beam is also illustrated in Figure 8c, where q is the weight distribution along the beam as $q = \pi \rho g R^2$, ρ is the density, g

is the gravitational acceleration, R is the radius of the beam, and L is the length of the beam, F_s is the maximum shear force $(\frac{1}{2}qL)$, and M_{max} is the maximum bending moment $(M_{max} = \frac{1}{8}qL^2)$.

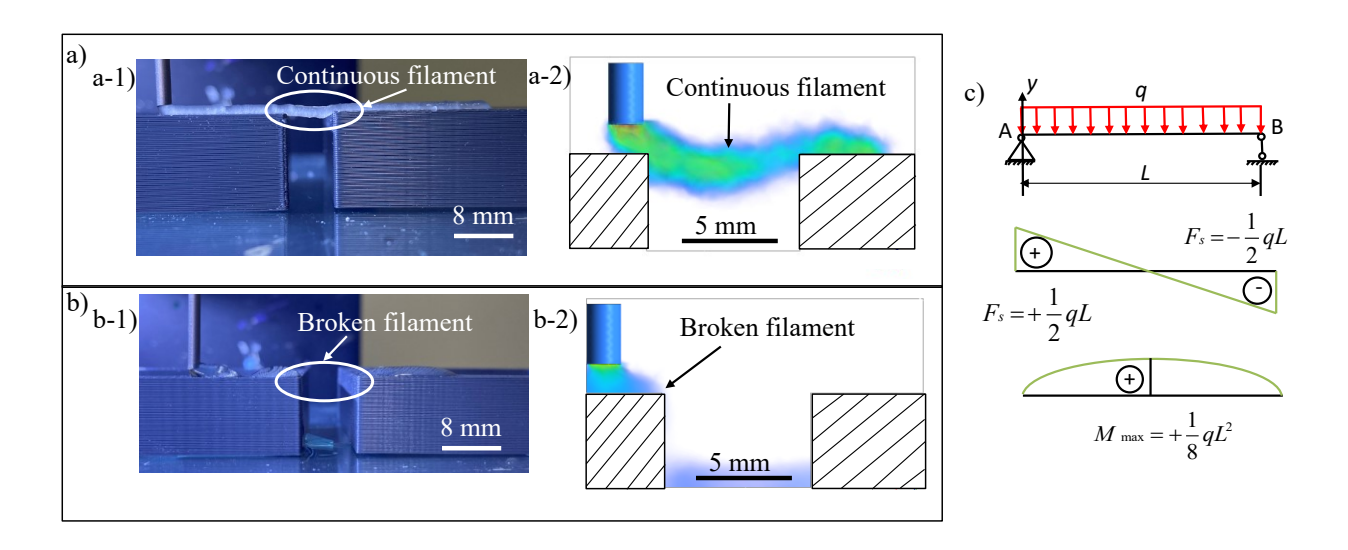


Figure 8. Printing of a simply supported beam. a-1) Experimental result and a-2) simulation result of the jammed gelatin microgel composite ink. b-1) Experimental result and b-2) simulation result of the gelatin solution. c) Mechanical model of a simply supported beam.

7.2 Cantilever filament printing

For printing of a cantilever beam, the jammed gelatin microgel composite ink can be deposited beyond a supporting substrate and hold itself in air as observed (Figure 9a-1) and simulated (Figure 9a-2). In contrast, the gelatin solution filament breaks once it leaves a supporting substrate as shown in Figure 9b-1 and 9b-2. The mechanics of such a cantilever beam is also illustrated in Figure 9c with $F_s = qL$ and $M_{\text{max}} = \frac{1}{2}qL^2$.

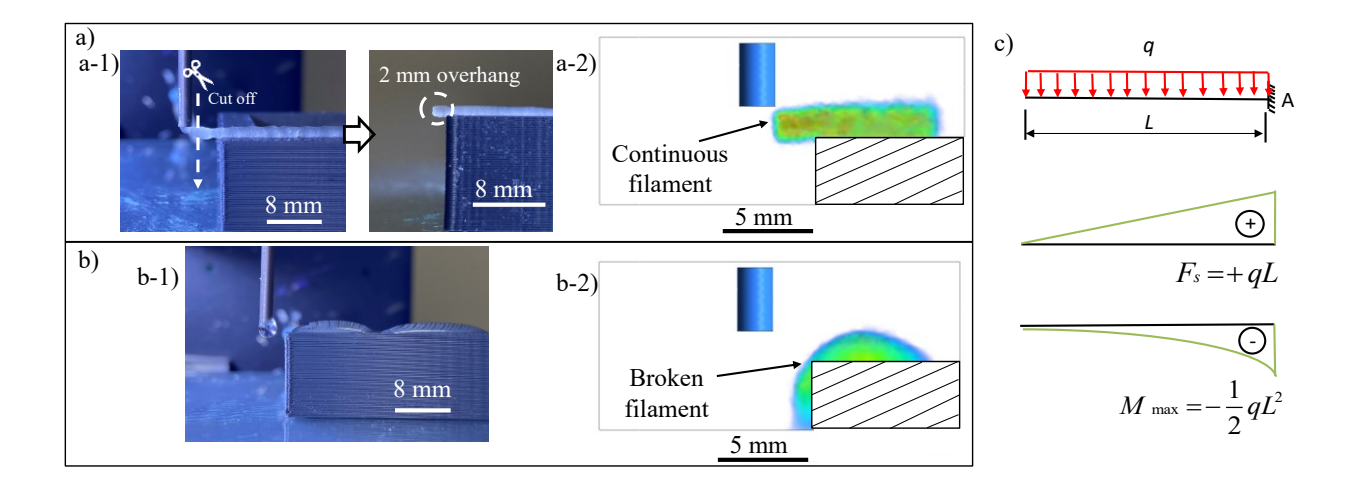


Figure 9. Printing of a cantilever beam. a-1) Experimental result and a-2) simulation result of the jammed gelatin microgel composite ink. b-1) Experimental result and b-2) simulation result of the gelatin solution. c) Mechanical model of a cantilever beam.

7.3 Evaluation of self-supported filament printability

The mechanical analysis was conducted to study the printable simply supported and cantilever beams/filaments when using the jammed gelatin microgel composite ink. For the simply supported beam model, the filament printed between two supporting substrates can be simplified as a beam with a uniformly distributed load by its own weight as shown in Figure 8c. The maximum shear stress τ_{\max} that always occurs at the two end points can be calculated by $\tau_{\max} = \frac{4F_s}{3A}$, where A is the cross-sectional area of the filament with $F_s = \frac{1}{2}qL$. As such, $\tau_{\max} = \frac{2}{3}\rho gL$. The maximum tensile stress that always occurs in the center of span can be calculated using $\sigma_{\max} = \frac{M_{\max}y}{I}$, where y is the distance between the neutral axis and analyzed surface, which equals to the radius of the filament (R) herein and I is the moment of inertia as $I = \frac{1}{4}\pi R^4$. Then the maximum tensile stress can be rewritten as: $\sigma_{\max} = \frac{\rho gL^2}{2R}$. To determine whether an overhang filament can be printed between two supporting substrates, the calculated maximum shear stress and maximum tensile stress are compared with the shear stress τ_{Ink} and tensile stress σ_{Ink} of the jammed microgel-

based composite ink. The ink tensile stress can be estimated by $\sigma_{ink} = \frac{3}{\sqrt{2}} \tau_{ink}$ according to the octahedral shear stress theory based on the ink shear stress at 25 °C, which is determined as 390.9 Pa based on the Herschel–Bulkley model. This results in a tensile stress value of 829.2 Pa. Then τ_{max} and σ_{max} are estimated as 52.27 Pa and 407.27 Pa, respectively (based on L=8 mm and R=0.77 mm herein), which are lower than τ_{ink} and σ_{ink} , so the filament does not break up during printing across an 8 mm span.

Similarly, for a cantilever beam with the filament printed beyond the supporting substrate, it can be simplified as a beam with a uniformly distributed weight-induced load (Figure 9c). The maximum shear stress that always occurs at the connection point can be calculated by $\tau_{\text{max}} = \frac{4F_s}{3A}$, and the maximum force occurring at the connection point is expressed as $F_s = qL$. As such, the maximum shear stress can be calculated as $\tau_{max} = \frac{4}{3}\rho gL$. The maximum tensile stress that occurs at the connection point can be calculated using $\sigma_{\text{max}} = \frac{M_{\text{max}}y}{I}$, which is $\sigma_{max} = \frac{2\rho gL^2}{R}$. To determine whether a cantilever or overhang filament can be printed beyond the supporting substrate, the calculated maximum shear stress and maximum tensile stress are compared to the shear stress τ_{ink} and tensile stress σ_{ink} of the composite ink. Then τ_{max} and σ_{max} of the cantilever beam are estimated to be 26.13 Pa and 101.82 Pa, respectively (based on L=2 mm and R=0.77 mm herein), which are lower than τ_{ink} and σ_{ink} , so the cantilever filament does not break up during deposition.

Furthermore, the achievable maximum length (without collapse) of the jammed gelatin microgel-based composite and gelatin solution inks, deposited both between two supporting substrates and over a supporting substrate, were simulated, and the results are shown in Figure 10a-1, 10a-2, 10b-1, and 10b-2. The maximum lengths are 12.6 mm and 6.3 mm for a simply supported beam and a cantilever beam, respectively, which are very close to the theoretical value (11.4 mm and 5.7 mm) (Figure 10c). When a structure with overhang features beyond these maximum lengths, the filaments collapse (Figure 10a-2 and 10b-2), and the structure design is inappropriate. It

demonstrates that the proposed computational approach can help better plan a printing process with satisfactory accuracy when using the jammed gelatin microgel composite ink.

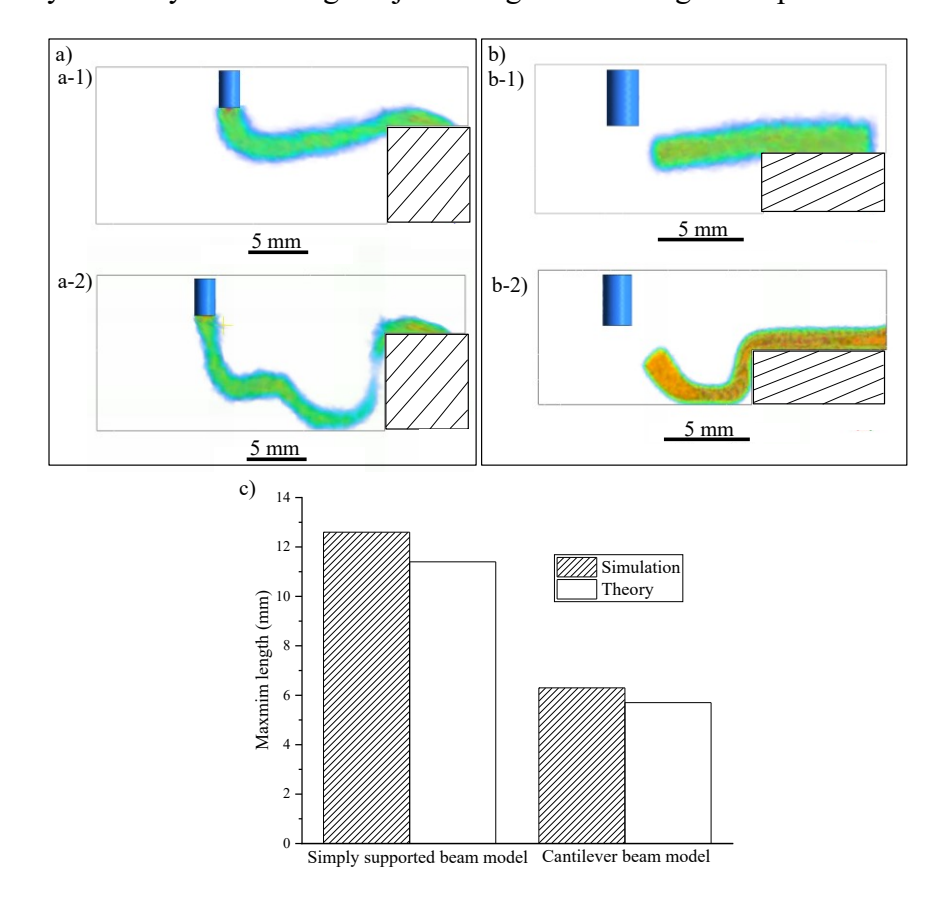


Figure 10. Prediction of maximum overhang length when printing a simply supported beam (a-1) deposition within the maximum length and (a-2) collapse when surpassing the maximum length. Prediction when printing a cantilever beam (b-1) deposition within the maximum length and (b-2) collapse when surpassing the maximum length. (c) Maximum length comparison between simulated and theoretical results.

8. Conclusions and future work

This research has computationally analyzed the printing process of the jammed gelatin microgel-based composite ink during extrusion printing in terms of the filament cross-sectional morphology and influence of the yield-stress fluid property on the structural printability. For the first time, the computational modeling of jammed gelatin microgel composite ink printing has been accomplished by using a fitted Herschel–Bulkley model to capture the constitutive behavior of the

microgel composite ink. As seen from the rheological measurements, the jammed gelatin microgel composite ink is a viscoplastic fluid with the shear-thinning property, and its yield-stress fluid property enables it for self-supported printing applications. The non-Newtonian Herschel–Bulkley model has been fitted based on the rheological measurements and further utilized to describe the constitutive behavior of the jammed gelatin microgel composite ink, which has resulted in good modeling performance in predicting the filament cross-sectional morphology under different printing conditions and estimating the achievable maximum length (without collapse) of the jammed gelatin microgel-based composite ink, deposited both between two supporting substrates and over a supporting substrate. It is found that the simplification of filament cross sections as elliptical or circular may not hold during the printing of the jammed microgel composite ink under a small normalized gap distance (less than 0.6) since the cross-sectional shape turns flat rectangular.

Future work may focus on analyzing other effects such as the printing temperature, nozzle shape, substrate material, and printing path on the filament cross-sectional morphology during extrusion printing of the jammed gelatin microgel composite ink and other types of non-Newtonian inks. The influence of additional living cells on the filament morphology should also be simulated for future biomedical applications. The improvement of the computational model which can simulate layer-by-layer structure printing processes and estimate the stress distribution within fabricated structures is also part of the future work. For practical process planning, the determination of the horizontal overlapping ratio between two adjacent filaments should be explored theoretically.

Competing financial interests

There are no competing financial interests.

Declaration of competing interest

One of the authors of this article is part of the editorial board of the journal. To avoid potential conflicts of interest, the responsibility for the editorial and peer-review process of this article lies with the journal's other editors. Furthermore, the authors of this article were removed from the peer review process and had no, and will not have any access to confidential information related to the editorial process of this article.

Acknowledgements

This study was partially supported by the US National Science Foundation (1762941), and the use of Anton Paar rheometer is acknowledged.

List of supporting information

Supporting Information M1: Movie of simulation of printing between two supporting substrates (Movie)

Supporting Information M2: Movie of printing between two supporting substrates. (Movie)

References:

- [1] S. V. Murphy, A. Atala, 3D bioprinting of tissues and organs, Nat. Biotechnol. 32 (2014) 773–785. https://doi.org/10.1038/nbt.2958.
- [2] Y. Huang, M.C. Leu, J. Mazumder, A. Donmez, Additive manufacturing: Current state, future potential, gaps and needs, and recommendations, J. Manuf. Sci. Eng. Trans. ASME. 137 (2015) 1–10. https://doi.org/10.1115/1.4028725.
- [3] Y. Huang, S.R. Schmid, Additive Manufacturing for Health: State of the Art, Gaps and Needs, and Recommendations, J. Manuf. Sci. Eng. Trans. ASME. 140 (2018) 1–11. https://doi.org/10.1115/1.4040430.
- [4] R. Xiong, Z. Zhang, W. Chai, Y. Huang, D.B. Chrisey, Freeform drop-on-demand laser printing of 3D alginate and cellular constructs, Biofabrication. 7 (2015). https://doi.org/10.1088/1758-5090/7/4/045011.
- [5] A. Sorkio, L. Koch, L. Koivusalo, A. Deiwick, S. Miettinen, B. Chichkov, H. Skottman, Human stem cell based corneal tissue mimicking structures using laser-assisted 3D bioprinting and functional bioinks, Biomaterials. 171 (2018) 57–71. https://doi.org/10.1016/j.biomaterials.2018.04.034.
- [6] C. Xu, W. Chai, Y. Huang, R.R. Markwald, Scaffold-free inkjet printing of three-dimensional zigzag cellular tubes, Biotechnol. Bioeng. 109 (2012) 3152–3160. https://doi.org/10.1002/bit.24591.
- [7] K. Christensen, C. Xu, W. Chai, Z. Zhang, J. Fu, Y. Huang, Freeform inkjet printing of cellular structures with bifurcations, Biotechnol. Bioeng. 112 (2015) 1047–1055. https://doi.org/10.1002/bit.25501.

- [8] D. Takagi, W. Lin, T. Matsumoto, H. Yaginuma, N. Hemmi, S. Hatada, M. Seo, High-precision three-dimensional inkjet technology for live cell bioprinting, Int. J. Bioprinting. 5 (2019) 27–38. https://doi.org/10.18063/ijb.v5i2.208.
- [9] Y. Jin, C. Liu, W. Chai, A. Compaan, Y. Huang, Self-Supporting Nanoclay as Internal Scaffold Material for Direct Printing of Soft Hydrogel Composite Structures in Air, ACS Appl. Mater. Interfaces. 9 (2017) 17456–17465. https://doi.org/10.1021/acsami.7b03613.
- [10] Y. Jin, A. Compaan, W. Chai, Y. Huang, Functional Nanoclay Suspension for Printing-Then-Solidification of Liquid Materials, ACS Appl. Mater. Interfaces. 9 (2017) 20057– 20066. https://doi.org/10.1021/acsami.7b02398.
- [11] W. Liu, Y.S. Zhang, M.A. Heinrich, F. De Ferrari, H.L. Jang, S.M. Bakht, M.M. Alvarez, J. Yang, Y.C. Li, G. Trujillo-de Santiago, A.K. Miri, K. Zhu, P. Khoshakhlagh, G. Prakash, H. Cheng, X. Guan, Z. Zhong, J. Ju, G.H. Zhu, X. Jin, S.R. Shin, M.R. Dokmeci, A. Khademhosseini, Rapid Continuous Multimaterial Extrusion Bioprinting, Adv. Mater. 29 (2017) 1–8. https://doi.org/10.1002/adma.201604630.
- [12] K. Song, A.M. Compaan, W. Chai, Y. Huang, Injectable Gelatin Microgel-Based Composite Ink for 3D Bioprinting in Air, ACS Appl. Mater. Interfaces. 12 (2020) 22453–22466. https://doi.org/10.1021/acsami.0c01497.
- [13] M.P. Lutolf, J.A. Hubbell, Synthetic biomaterials as instructive extracellular microenvironments for morphogenesis in tissue engineering, Nat. Biotechnol. 23 (2005) 47–55. https://doi.org/10.1038/nbt1055.
- [14] M.W. Tibbitt, K.S. Anseth, Hydrogels as extracellular matrix mimics for 3D cell culture, Biotechnol. Bioeng. 103 (2009) 655–663. https://doi.org/10.1002/bit.22361.
- [15] S.R. Caliari, J.A. Burdick, A practical guide to hydrogels for cell culture, Nat. Methods. 13 (2016) 405–414. https://doi.org/10.1038/nmeth.3839.
- [16] N. Gjorevski, N. Sachs, A. Manfrin, S. Giger, M.E. Bragina, P. Ordóñez-Morán, H. Clevers, M.P. Lutolf, Designer matrices for intestinal stem cell and organoid culture, Nature. 539 (2016) 560–564. https://doi.org/10.1038/nature20168.
- [17] L. Moroni, J.A. Burdick, C. Highley, S.J. Lee, Y. Morimoto, S. Takeuchi, J.J. Yoo, Biofabrication strategies for 3D in vitro models and regenerative medicine, Nat. Rev. Mater. 3 (2018) 21–37. https://doi.org/10.1038/s41578-018-0006-y.
- [18] Z. Zhang, Y. Jin, J. Yin, C. Xu, R. Xiong, K. Christensen, B.R. Ringeisen, D.B. Chrisey,

- Y. Huang, Evaluation of bioink printability for bioprinting applications, Appl. Phys. Rev. 5 (2018). https://doi.org/10.1063/1.5053979.
- [19] C.B. Highley, K.H. Song, A.C. Daly, J.A. Burdick, Jammed Microgel Inks for 3D Printing Applications, Adv. Sci. 6 (2019). https://doi.org/10.1002/advs.201801076.
- [20] M. Shin, K.H. Song, J.C. Burrell, D.K. Cullen, J.A. Burdick, Injectable and Conductive Granular Hydrogels for 3D Printing and Electroactive Tissue Support, Adv. Sci. 6 (2019) 1–8. https://doi.org/10.1002/advs.201901229.
- [21] R.J. Ketz, R.K. Prud'homme, W.W. Graessley, Rheology of concentrated microgel solutions, Rheol. Acta. 27 (1988) 531–539. https://doi.org/10.1007/BF01329353.
- [22] J.L. Andrea, R.N. Sindey, Jamming is not just cool any more, Nature. 81 (1998) 226–231. www.nature.com.
- [23] C.S. O'Hern, L.E. Silbert, A.J. Liu, S.R. Nagel, Jamming at zero temperature and zero applied stress: The epitome of disorder, Phys. Rev. E Stat. Physics, Plasmas, Fluids, Relat. Interdiscip. Top. 68 (2003) 19. https://doi.org/10.1103/PhysRevE.68.011306.
- [24] P. Menut, S. Seiffert, J. Sprakel, D.A. Weitz, Does size matter? Elasticity of compressed suspensions of colloidal- and granular-scale microgels, Soft Matter. 8 (2012) 156–164. https://doi.org/10.1039/c1sm06355c.
- [25] Y. Li, J. Rodrigues, H. Tomás, Injectable and biodegradable hydrogels: Gelation, biodegradation and biomedical applications, Chem. Soc. Rev. 41 (2012) 2193–2221. https://doi.org/10.1039/c1cs15203c.
- [26] F. Jivan, R. Yegappan, H. Pearce, J.K. Carrow, M. McShane, A.K. Gaharwar, D.L. Alge, Sequential Thiol-Ene and Tetrazine Click Reactions for the Polymerization and Functionalization of Hydrogel Microparticles, Biomacromolecules. 17 (2016) 3516–3523. https://doi.org/10.1021/acs.biomac.6b00990.
- [27] Y. Yang, J. Zhang, Z. Liu, Q. Lin, X. Liu, C. Bao, Y. Wang, L. Zhu, Tissue-Integratable and Biocompatible Photogelation by the Imine Crosslinking Reaction, Adv. Mater. 28 (2016) 2724–2730. https://doi.org/10.1002/adma.201505336.
- [28] K. Su, C. Wang, Recent advances in the use of gelatin in biomedical research, Biotechnol. Lett. 37 (2015) 2139–2145. https://doi.org/10.1007/s10529-015-1907-0.
- [29] X. Wang, Q. Ao, X. Tian, J. Fan, H. Tong, W. Hou, S. Bai, Gelatin-based hydrogels for organ 3D bioprinting, Polymers (Basel). 9 (2017). https://doi.org/10.3390/polym9090401.

- [30] R. Anitha, S. Arunachalam, P. Radhakrishnan, Critical parameters influencing the quality of prototypes in fused deposition modelling, J. Mater. Process. Technol. 118 (2001) 385–388. https://doi.org/10.1016/S0924-0136(01)00980-3.
- [31] J.F. Rodriguez, J.P. Thomas, J.E. Renaud, Characterization of the mesostructure of fused-deposition acrylonitrile-butadiene-styrene materials, Rapid Prototyp. J. 6 (2000) 175–185. https://doi.org/10.1108/13552540010337056.
- [32] C. Bellehumeur, L. Li, Q. Sun, P. Gu, Modeling of bond formation between polymer filaments in the fused deposition modeling process, J. Manuf. Process. 6 (2004) 170–178. https://doi.org/10.1016/S1526-6125(04)70071-7.
- [33] Q. Sun, G.M. Rizvi, C.T. Bellehumeur, P. Gu, Effect of processing conditions on the bonding quality of FDM polymer filaments, Rapid Prototyp. J. 14 (2008) 72–80. https://doi.org/10.1108/13552540810862028.
- [34] L. Li, Q. Sun, C. Bellehumeur, P. Gu, Composite modeling and analysis for fabrication of FDM prototypes with locally controlled properties, J. Manuf. Process. 4 (2002) 129–141. https://doi.org/10.1016/S1526-6125(02)70139-4.
- [35] C. Ziemian, M. Sharma, S. Ziemi, Anisotropic Mechanical Properties of ABS Parts Fabricated by Fused Deposition Modelling, Mech. Eng. 23 (2012). https://doi.org/10.5772/34233.
- [36] E. Bertevas, J. Férec, B.C. Khoo, G. Ausias, N. Phan-Thien, Smoothed particle hydrodynamics (SPH) modeling of fiber orientation in a 3D printing process, Phys. Fluids. 30 (2018). https://doi.org/10.1063/1.5047088.
- [37] Q. Liu, N. Zhang, W. Wei, X. Hu, Y. Tan, Y. Yu, Y. Deng, C. Bi, L. Zhang, H. Zhang, Assessing the dynamic extrusion-based 3D printing process for power-law fluid using numerical simulation, J. Food Eng. 275 (2020) 109861. https://doi.org/10.1016/j.jfoodeng.2019.109861.
- [38] J. Du, Z. Wei, X. Wang, J. Wang, Z. Chen, An improved fused deposition modeling process for forming large-size thin-walled parts, J. Mater. Process. Technol. 234 (2016) 332–341. https://doi.org/10.1016/j.jmatprotec.2016.04.005.
- [39] A. D'Amico, A.M. Peterson, An adaptable FEA simulation of material extrusion additive manufacturing heat transfer in 3D, Addit. Manuf. 21 (2018) 422–430. https://doi.org/10.1016/j.addma.2018.02.021.

- [40] B. Brenken, E. Barocio, A. Favaloro, V. Kunc, R.B. Pipes, Development and validation of extrusion deposition additive manufacturing process simulations, Addit. Manuf. 25 (2019) 218–226. https://doi.org/10.1016/j.addma.2018.10.041.
- [41] A. Gleadall, I. Ashcroft, J. Segal, VOLCO: A predictive model for 3D printed microarchitecture, Addit. Manuf. 21 (2018) 605–618. https://doi.org/10.1016/j.addma.2018.04.004.
- [42] R. Comminal, M.P. Serdeczny, D.B. Pedersen, J. Spangenberg, Numerical modeling of the strand deposition flow in extrusion-based additive manufacturing, Addit. Manuf. 20 (2018) 68–76. https://doi.org/10.1016/j.addma.2017.12.013.
- [43] M.R. Talagani, S. Dormohammadi, R. Dutton, C. Godines, H. Baid, F. Abdi, Numerical simulation of big area additive manufacturing (3D printing) of a full size car, (2015) 27–36.
- [44] Y. Xu, H. Zhang, B. Šavija, S. Chaves Figueiredo, E. Schlangen, Deformation and fracture of 3D printed disordered lattice materials: Experiments and modeling, Mater. Des. 162 (2019) 143–153. https://doi.org/10.1016/j.matdes.2018.11.047.
- [45] M.P. Serdeczny, R. Comminal, D.B. Pedersen, J. Spangenberg, Experimental validation of a numerical model for the strand shape in material extrusion additive manufacturing, Addit. Manuf. 24 (2018) 145–153. https://doi.org/10.1016/j.addma.2018.09.022.
- [46] J.F. Agassant, F. Pigeonneau, L. Sardo, M. Vincent, Flow analysis of the polymer spreading during extrusion additive manufacturing, Addit. Manuf. 29 (2019) 100794. https://doi.org/10.1016/j.addma.2019.100794.
- [47] F. Liravi, R. Darleux, E. Toyserkani, Additive manufacturing of 3D structures with non-Newtonian highly viscous fluids: Finite element modeling and experimental validation, Addit. Manuf. 13 (2017) 113–123. https://doi.org/10.1016/j.addma.2016.10.008.
- [48] R. Comminal, J.H. Hattel, J. Spangenberg, Numerical Simulations of Planar Extrusion and Fused Filament Fabrication of Non-Newtonian Fluids, Annu. Trans. Nord. Rheol. Soc. (2017). https://nrs.blob.core.windows.net/pdfs/nrspdf-5d42483a-2eeb-43ec-b4ab-a1614ac62fla.pdf.
- [49] D. Chimene, C.W. Peak, J.L. Gentry, J.K. Carrow, L.M. Cross, E. Mondragon, G.B. Cardoso, R. Kaunas, A.K. Gaharwar, Nanoengineered Ionic-Covalent Entanglement (NICE) Bioinks for 3D Bioprinting, ACS Appl. Mater. Interfaces. 10 (2018) 9957–9968.

- https://doi.org/10.1021/acsami.7b19808.
- [50] A.A. Adib, D.J. Hoelzle, Hybrid Control of Flowrate in Microextrusion-Based Direct-Write Additive Manufacturing, IEEE Control Syst. Lett. 1456 (2021). https://doi.org/10.1109/LCSYS.2021.3049897.
- [51] K. Lee, Y. Chen, X. Li, Y. Wang, N. Kawazoe, G. Chen, K. Lee, Y. Chen, Y. Wang, G. Chen, X. Li, Y. Yang, Solution viscosity regulates chondrocyte proliferation and phenotype during 3D culture, J. Mater. Chem. B. 7 (2019) 7713–7722. https://doi.org/10.1039/c9tb02204j.
- [52] R. Wulansari, J.R. Mitchell, J.M.V. Blanshard, J.L. Paterson, Why are gelatin solutions Newtonian? Food Hydrocoll. 12 (1998) 245–249. https://doi.org/10.1016/S0268-005X(98)00038-1.
- [53] L. Riley, L. Schirmer, T. Segura, Granular hydrogels: emergent properties of jammed hydrogel microparticles and their applications in tissue repair and regeneration, Curr. Opin. Biotechnol. 60 (2019) 1–8. https://doi.org/10.1016/j.copbio.2018.11.001.
- [54] E.R. Weeks, Soft jammed materials, Stat. Phys. Complex Fluids. (2007) 1–87. http://laplace.ucv.cl/Patterns/Referencias/soft-materials-sendai2007.pdf.
- [55] D. M. Cruz, J. L. Ivirico, Manuela M. Gomes, J. L. Ribelles, M. Salmerón Sánchez, R. L. Reis, and J. F. Mano. "Chitosan microparticles as injectable scaffolds for tissue engineering." Tissue Engineering. Part A 14, no. 5 (2008) 821-821.
- [56] S.F. Costa, F.M. Duarte, J.A. Covas, Towards modelling of Free Form Extrusion: Analytical solution of transient heat transfer, Int. J. Mater. Form. 1 (2008) 703–706.